

Electromagnetic Field Safety Analysis of a 7.7 kW Wireless Power Transfer System for Electric Vehicles

Songtao Liu¹, Deguan Li¹, Chuanmin Chen^{1, *},
Wenbo Jia¹, Kai Che², and Jinxing Yu²

Abstract—The safety of the electromagnetic environment of wireless power transfer (WPT) systems is one of the prerequisites for the application of wireless charging technology for electric vehicles (EVs). The electromagnetic characteristics of a wireless charging EV with a new 7.7 kW WPT system were modeled and analyzed in this paper. Firstly, a complete model of the magnetic coupler was built as a source of electromagnetic radiation, and an external excitation source was added by coupling the resonant coils to the double inductor-capacitor-capacitor (LCC-LCC) topology circuit model. Secondly, the finite element analysis software COMSOL Multiphysics was used to solve for the magneto-quasi-static values to verify the electromagnetic safety of the wireless charging process. Then, two charging scenarios were investigated when the GA and VA aligned and misaligned, involving lateral offset and longitudinal offset cases. Finally, the simulation results were compared and analyzed, showing that the values of electromagnetic fields become higher as the offset distance increases. In worst-case scenarios, the highest magnetic flux density (1.1 μT) is observed in the virtual plane of the test on the left side of the vehicle, which occupies only 17.6% of the limits specified in ICNIRP 1998 (6.25 μT), indicating a good EMF safety performance of the wireless charging system.

1. INTRODUCTION

The extensive promotion and use of electric vehicles (EVs) have created a huge demand for charging. Nowadays, EV battery charging is carried out via the plug-in (conductive) connection. Along with the development of autonomous driving technology, there are new requirements for automated charging of onboard batteries, where the charging process does not require any human intervention. Wireless power transfer (WPT) is an appropriate solution for this goal soon [1–3].

Among near-field coupling WPT technologies, the magnetic resonant coupling (MRC) WPT is advantageous for its long transmission distance and is less susceptible to the influence of certain metals in the transmission channel, which is considered more suitable for wireless charging of electric vehicles (EVs) [4–8]. The MCR-WPT relies on two or more electromagnetic resonant systems with the same resonant frequency and high factor quality to complete the wireless transmission of electrical energy through high-frequency alternating magnetic energy conversion [9]. However, due to the loose coupling between the two sides, the system may result in a large amount of electromagnetic field (EMF) emissions in and around the vehicle, and leaking EMF emissions can be a serious safety concern [10]. Ensuring that EMF emissions are kept below EMF safety limits is one of the prerequisites for the application of wireless charging technology for EVs. The standards for wireless charging of EVs have recommended the guideline of the International Commission of Non-Ionized Radiation Protection (ICNIRP) for the assessment of the electromagnetic safety performance of WPT [8, 11–13]. The ICNIRP Guidelines

Received 4 March 2023, Accepted 29 April 2023, Scheduled 14 May 2023

* Corresponding author: Chuanmin Chen (hdccm@126.com).

¹ Department of Environmental Science and Engineering, North China Electric Power University, Baoding 071003, China. ² State Grid Hebei Electric Power Co., Ltd, Shijiazhuang 050000, China.

established electric and magnetic field exposure limits ranging from 1 Hz to 10 MHz for the general public and occupational exposure [14], and the safety limits in terms of the magnetic flux density at the operational nominal frequency $f_0 = 85$ kHz (tuning band 81.38 to 90 kHz) were $6.25 \mu\text{T}$ for ICNIRP 1998 and $27 \mu\text{T}$ for ICNIRP 2010.

In terms of electromagnetic exposure safety, several pertinent studies were carried out by many researchers to analyze the electromagnetic field radiation during the wireless charging of EVs. Reference [15] evaluated the EMF emissions of a WPT EV under different exposure conditions, but only the WPT system was taken into account in the analysis, and the car body was not. In [16], the electromagnetic exposure of a carbon fiber EV with an output of 7.7 kW was explored under the most unfavorable conditions of misalignment of the transmitting and receiving coils. A small portion of the driver's foot exceeded the ICNIRP limits. The vehicle body and body materials were considered in the analysis, but the WPT system model was over-simplified, and the shielding effect of the coupler itself was not fully considered. Reference [17] took the MCR-WPT of an EV as the electromagnetic exposure source, and the electromagnetic field strength of the human tissue at the observation point outside the EV was simulated and calculated in the wireless charging of the EV under different shielding conditions. The comparison results showed that the maximum B and E values adding metal shielding in the horizontal direction were lower than those specified in the exposure limits set by the ICNIRP. In summary, the magnetic coupler is often considered to be a source of electromagnetic exposure when studying the safety of electromagnetic fields for wireless charging in electric vehicles, but the simulation model is not yet complete. The shielding effect of the vehicle body also needs to be taken into account fully, so a complete vehicle body model needs to be constructed.

In addition, the new compensation network topology, such as bilateral inductor-capacitor-capacitor (LCC), has been shown to keep fluctuations in the magnetic coupling coefficient within acceptable limits during physical excursions of the magnetic coupler and can effectively improve the magnetic field balance. Therefore, a comprehensive consideration of the application of new coupling structures is very important for the electromagnetic radiation characteristics of wireless charging for EVs.

The safety of the EMF during wireless charging for the driver and passengers in the vehicle or pedestrians nearby is one of the fundamental issues that need to be addressed before WPT technology is commercially available after several years. The EMF of wireless charging EVs with a new 7.7 kW WPT system is numerically predicted in this paper. As the main focus is on assessing the magnetic field in the environment, the relatively complete magnetic coupling model containing copper coil, ferrite magnetic core, and aluminium shield plate was also considered in this article. In addition, this paper focuses on the EMF distribution at maximum ground clearance and maximum offset between the ground assembly (GA) and the vehicle assembly (VA). The computed results were compared with the limits prescribed in the standards established by the ICNIRP to evaluate the EMF safety performance of the WPT system.

2. WPT OPERATION SCENARIO ANALYSIS AND SIMULATION MODEL

2.1. WPT Operating Scenario Analysis

In general application scenarios, the GA is fixed on the ground, and the VA is mounted under the EV chassis. The vertical separation (air gap) between GA and VA, which is generally constrained by the height of the vehicle chassis, plays an important role in the level of the magnetic field generated by the automotive WPT system. Three Z -classes are defined to classify the WPT systems based on the maximum ground clearance as $Z1 = 100\text{--}150$ mm, $Z2 = 140\text{--}210$ mm, and $Z3 = 170\text{--}250$ mm. In addition, the operation of the GA and VA offset in the horizontal direction should also be considered. For this reason, it is difficult for the user to place the onboard receiver in the optimal position, where the GA and VA center points coincide with each other. The offset errors between GA and VA are inevitable, especially without the assistance of a positioning device. Application in the actual charging, the admissible offset errors allowed by the SAE Recommended Practice (RP) J2954 [8], as shown in Fig. 1, the maximum offset in the fore and aft direction (X axis) and lateral direction (Y axis) are ± 100 mm (ΔX_{\max}) and ± 75 mm (ΔY_{\max}), respectively. Furthermore, the efficiency is also standardized: $> 85\%$ for aligned coils, and $> 80\%$ for misaligned coils (offset position).

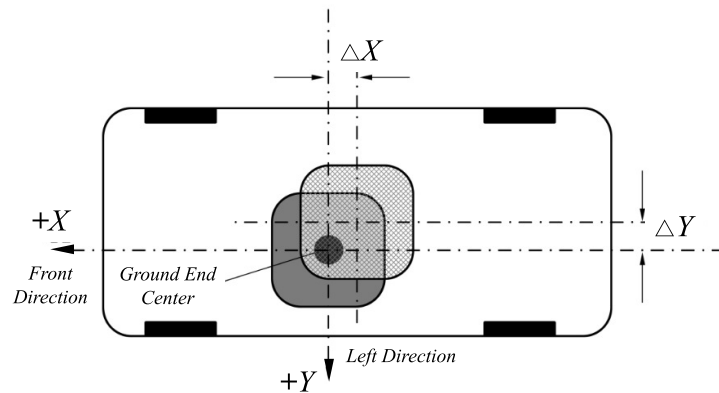


Figure 1. Offset scenario diagram.

The coupling factor k between coils reflects the energy transfer performance, which depends on the coil design, the separation distance between the coils, and their possible lateral misalignment [10]. While the value of k decreases when there is an offset between wireless charging systems, the current in the transmitting coil is coordinated to rise to maintain effective energy transmission, and as a result, the EMF leakage in the environment can be very high. To ensure EM safety under the worst case, those scenarios need to be investigated.

2.2. Magnetic Coupled Resonator Simulation Model

An exemplary WPT system was designed with a reference to GB/T 38775 (in Chinese) [18, 19] and simulated to calculate the magnetic field emission. The model structure of the wireless power transfer system is shown in Fig. 2. It was designed to operate at the WPT2 power level (7.7 kW) and maximum ground clearance Z1 (100–150 mm). The VA coil is a double-winding planar coil instead of a Double-D (DD) coil, and the GA coil is a single-turn planar coil. The ferrite core between the planar coil and the aluminium shield can concentrate the field, and its simulation model is shaped as a complete rectangular

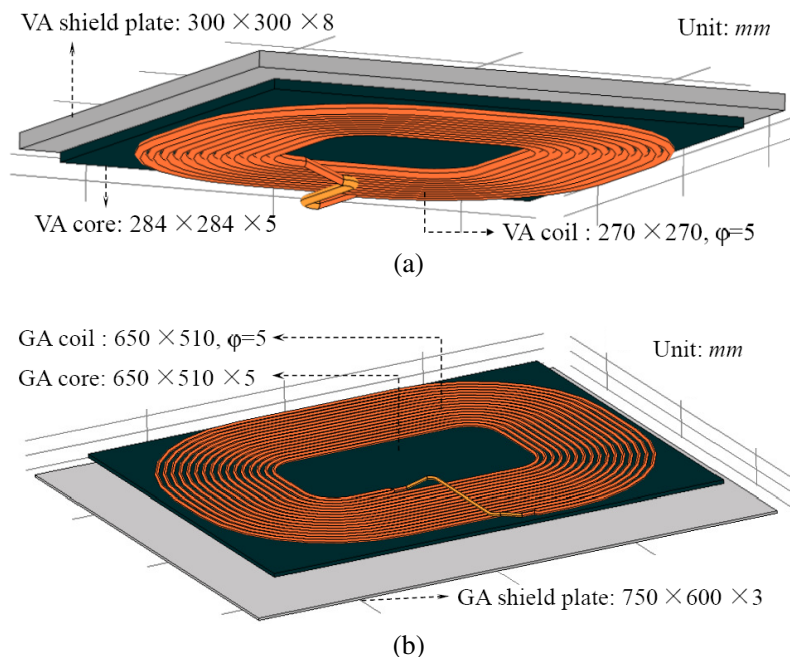


Figure 2. Simulation models of (a) the VA and (b) the GA of the WPT2-Z1 system.

Table 1. Relevant parameters of materials.

Component	Size (mm)	Material	Conductivity (S/m)
VA shield plate	$300 \times 300 \times 8.0$	Aluminum 3003	$2.3 \cdot 10^7$
VA core	$284 \times 284 \times 5.0$	Ferrite	5
VA coil	$270 \times 270, \varphi 5.0$ (2 × 8 turns)	Copper	$6.0 \cdot 10^7$
GA coil	$650 \times 500, \varphi 5.0$ (10 turns)	Copper	$6.0 \cdot 10^7$
GA core	$650 \times 510 \times 5.0$	Ferrite	5
GA shield plate	$750 \times 600 \times 3.0$	Aluminum 3003	$2.3 \cdot 10^7$

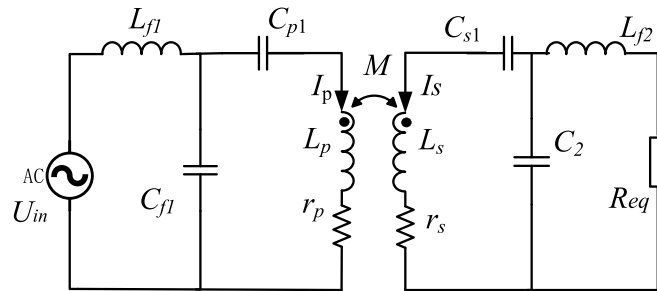
plate rather than many small pieces interlaced. The materials and related parameters used for each component are shown in Table 1.

The air gap between different components is necessary, which is determined by the electrical performance of the WPT system. The air gap between the coil and ferrite core is 1.0 mm in both assemblies, and that between the core and the shield is 3.0 mm and 30 mm in the VA and GA, respectively.

2.3. Compensation Circuit Model of WPT System

The design of the compensation network of the WPT system is an important way to improve anti-offset performance [20–23]. The current can be self-adjusted when the k changes, and the power can be maintained in a controlled fluctuation range by reasonably designing the compensation network parameters.

The topological structure of the bilateral LCC WPT system analyzed in this paper is shown in Fig. 3. The high-frequency AC voltage source U_{in} on the primary side is generated by the high-frequency inverter and used as the input source of the compensation network on the primary side [22]. After the power is transmitted through the LCC-LCC WPT system, it is then received by the VA coil to supply power to the resistive load. The compensation network parameters are listed in Table 2.

**Figure 3.** LCC compensation topology for WPT.

2.4. Finite Element Simulation Model of Wireless Charging EV

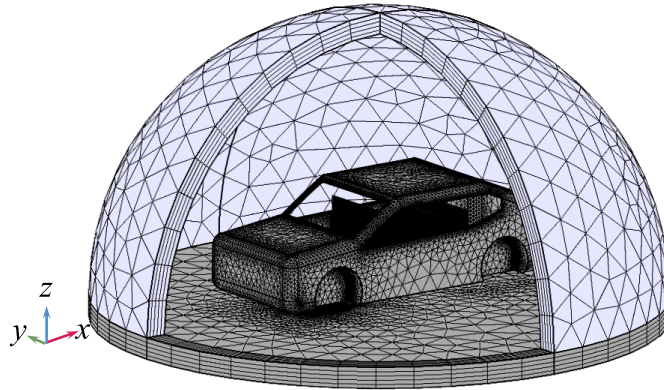
To efficiently perform simulations and adequately capture the characterization of the EMF distribution, a finite element simulation model of wireless charging is constructed. The considered car outer dimensions are: $l_x = 480$ cm, $l_y = 185$ cm, and $l_z = 133$ cm (without wheels), and the thickness of the car body is 5 mm. The car shell is assumed to be steel, and conductivity $\sigma = 1.12 \cdot 10^7$ S/m.

The distance of the car platform from the ground is set to 17 cm, which meets the installation conditions for the WPT2-Z1 constructed in Section 2.2, with an air gap of 150 mm between the GA and VA coils. To simulate the offset situation discussed in Section 2.1, the relative positions of GA and VA can be changed.

Table 2. Relevant parameters of materials.

Parameter	Value	Parameter Explaining
U_{in}	477.8 VAC	GA source voltage
L_{f1}	22.0 μ H	GA compensation inductance
C_{p1}	130.5 nF	GA parallel compensation capacitor
C_{f1}	157.9 nF	GA series compensation capacitor
r_p	7.2 m Ω	the internal resistance of the GA coil
L_p	42.4 μ H	self-inductance of the GA coil
L_s	42.0 μ H	self-inductance of the VA coil
r_s	12.5 m Ω	the internal resistance of the VA coil
C_{s1}	120.8 nF	VA series compensation capacitor
C_2	268.1 nF	VA parallel compensation capacitor
L_{f2}	13.0 μ H	VA compensation inductance
R_{eq}	10.8 Ω	equivalent resistive load
f	85.5 kHz	the operational frequency of the WPT

Fig. 4 shows the total tetrahedral meshes diagram of the finite element simulation model. A spherical external boundary with magnetic and electric insulation is used to simulate the free space at the simulation domain's edge. The magnetic and electric insulation condition is sufficient in this case since the propagating wave components are insignificant at the boundary compared to them in the simulation domain's center.

**Figure 4.** Meshing diagram of the finite element simulation model.

3. NUMERICAL ANALYSIS METHOD

In theory, the magnetic field in a wireless charging scenario can be calculated in the frequency domain by solving the magneto-quasi static (MQS) equations. The finite element analysis software COMSOL Multiphysics was used to solve for the magneto-quasi-static values, and the relevant equations are calculated as follows.

$$\nabla \times H = J + \frac{\partial D}{\partial t} = J \quad (1)$$

$$\nabla \times E = -\frac{\partial B}{\partial t} \quad (2)$$

$$\nabla \cdot D = \rho \quad (3)$$

$$\nabla \times B = 0 \quad (4)$$

where H (A/m) is the magnetic field strength, J (A/m²) the current density, D (C/m²) the electric flux density, E (V/m) the electric field strength, B (T) the magnetic flux density, and ρ (C/m³) the charge density. In addition, the constitutive relation has the following three equations.

$$B = \mu H \quad (5)$$

$$D = \varepsilon_0 \varepsilon_r E \quad (6)$$

$$J = \sigma E \quad (7)$$

where ε_0 (F/m) is the dielectric constant of vacuum, with the value of 8.85×10^{-12} ; ε_r (dimensionless) is the relative dielectric constant; and σ (S/m) is the electrical conductivity.

In this study, the electromagnetic field interface based on (1)–(7) under the AC/DC module of COMSOL v5.6 is used, which is proved to be an effective simulation tool for EM problems. In addition, the circuit interface is constructed regarding the equivalent circuit model in Section 2.3 and coupled to the transmitting and receiving coils respectively as external excitation sources for the magnetic coupler.

4. RESULTS AND DISCUSSION

As described in the standards of the EMF safety of wireless charging EVs, the protected areas are mainly divided into three areas. The area around the magnetically coupled resonator and underneath the vehicle's chassis, which is denoted as the area 1, is where energy is transferred. Area 2 is the region surrounding the vehicle from the ground to the roof. As shown in Fig. 5(a), the X - Z and Y - Z planes serve as the virtual planes for EMF measurements, and the test point is located there at a horizontal distance of 20 cm from the vehicle surface (except for the rearview, the most prominent edge of the vehicle body is the starting point). Area 3 is the interior space of the vehicle, and the EMF test is for the passenger seats, as shown in Fig. 5(b), with test points located 10 mm above the head, chest, seat cushion, and foot.

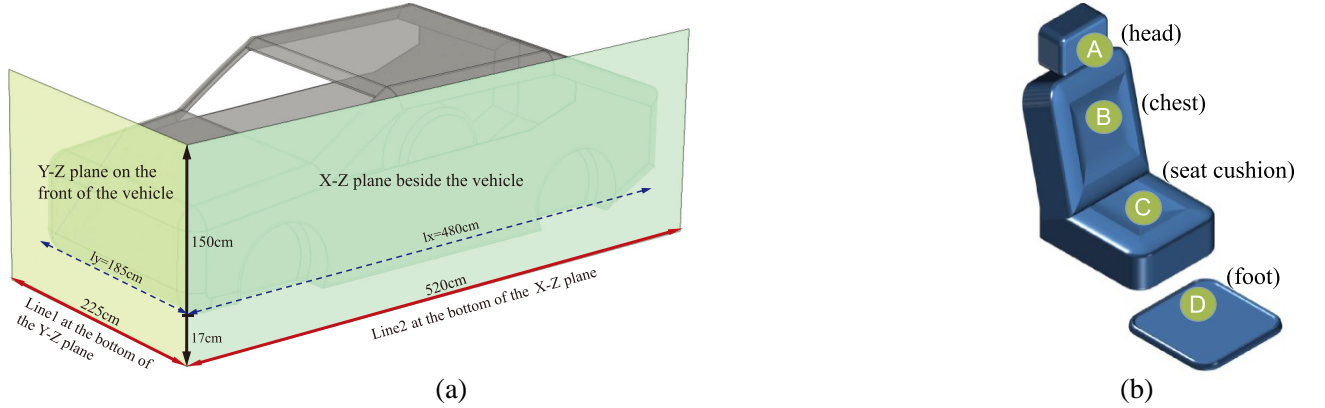


Figure 5. EMF verification test points in (a) protection area 2 and (b) protection area 3.

4.1. Distribution of the Magnetic Field around the WPT System

The EMF distribution of the wireless charging EV is simulated based on the MQS equations solved in Section 3. In this example, the coils spacing $Z1 = 150$ mm and $\Delta X = \Delta Y = 0$. The magnetic field distribution around the WPT system on the center section plane is shown in Fig. 6(a). It can be seen that a relatively inhomogeneous magnetic field from the WPT system was caused by the shielding plates and chassis of the car. Further, due to the shielding effect of the car body, the magnetic field strength inside the car is less than that outside. Fig. 6(b) illustrates the magnetic field distribution on the region between coils under the vehicle. The magnetic field is concentrated around the wireless charging system, and the magnetic field strength in the energy transfer area is high, far exceeding the

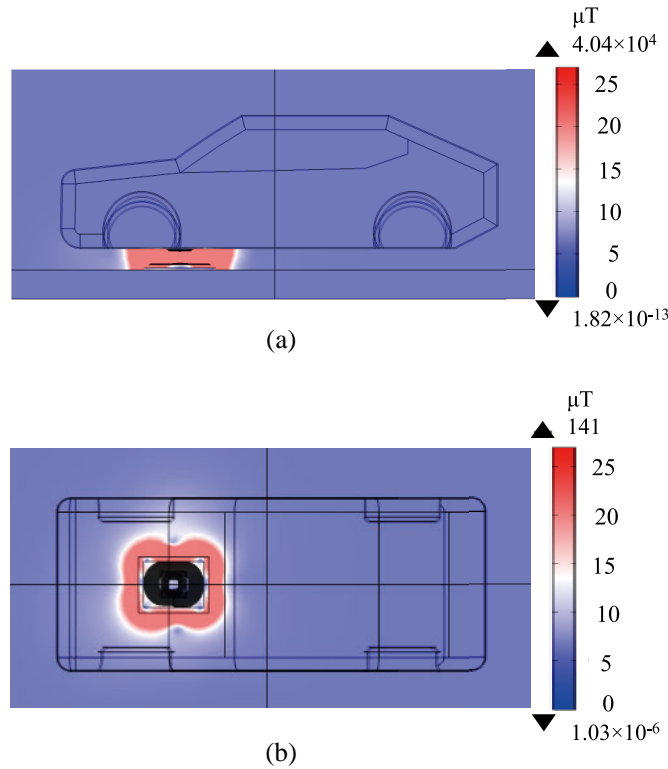


Figure 6. Magnetic flux density distributions around the WPT system on (a) the center section plane (side view) and (b) the plane under the car between coils (top view) when the GA and VA aligned.

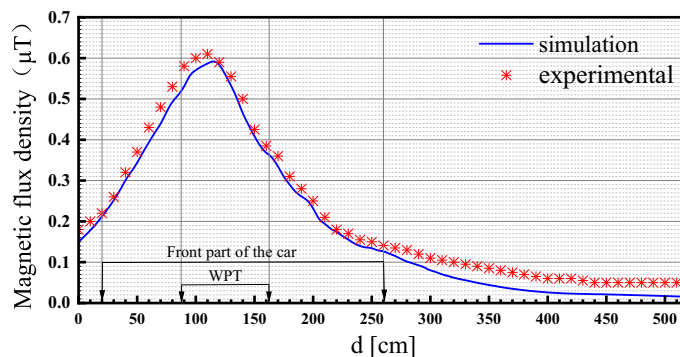


Figure 7. Magnetic flux experimental and simulation results on line 2.

safety limits required in ICNIRP guidelines. The electromagnetic exposure hazards to humans in area 1 must be prevented, and the charging process should be stopped in time to avoid exposure to organisms through control access techniques. Therefore, protection area 1 was excluded, and the EMF safety was chosen to be verified for the test planes discussed in area 2 and area 3.

The reliability of the simulation model was verified by comparing the experimental measurements. The EV used for the experimental test was equipped with an MF-WPT2-Z1 WPT system designed with reference to the GB/T 38775 (in Chinese) series of standards, with an output power of 6.9 kW and an optimum efficiency of 89.6%. The experimental prototype is adjusted to a good working state, and the magnetic flux measurement is carried out under the condition of coil alignment. In order to better analyze the error situation between the simulation and measurement results, a reference line of length 520 cm is made, as shown in Fig. 5(a), with a line 2 located at the bottom of the X - Z virtual

plane and each measurement point position spaced at 10 cm. The experimental and simulated results are shown in Fig. 7. It can be seen that the simulation results on line 2 are in good agreement with the measurement data. However, the simulation results are in general lower than the measured ones, presumably because the experimental measurements are influenced by the background values of the electromagnetic environment. Comparing the relative error between the simulation and measurement results, the simulation error is 9.59% corresponding to the first half of the car body ($d = 20\text{--}260\text{ cm}$), so the simulation model is reliable.

4.2. EMF Safety Verification and Analysis

For each offset case, the simulation was carried out several times using similar meshes to evaluate the distribution of the magnetic field in the measuring areas of an EV during wireless charging. In the case of positive alignment of GA and VA, the EMF distribution outside the wireless charging EV is shown in Fig. 8. From the analysis of the magnetic field distributions around the wireless charging EV on the $Y\text{-}Z$ plane and $X\text{-}Z$ plane, it can be seen that the magnetic field is mainly concentrated in the front half of the car body, and the maximum value of the magnetic field obtained in both measurement planes is $0.57\ \mu\text{T}$, which is much lower than the EMF safety limit.

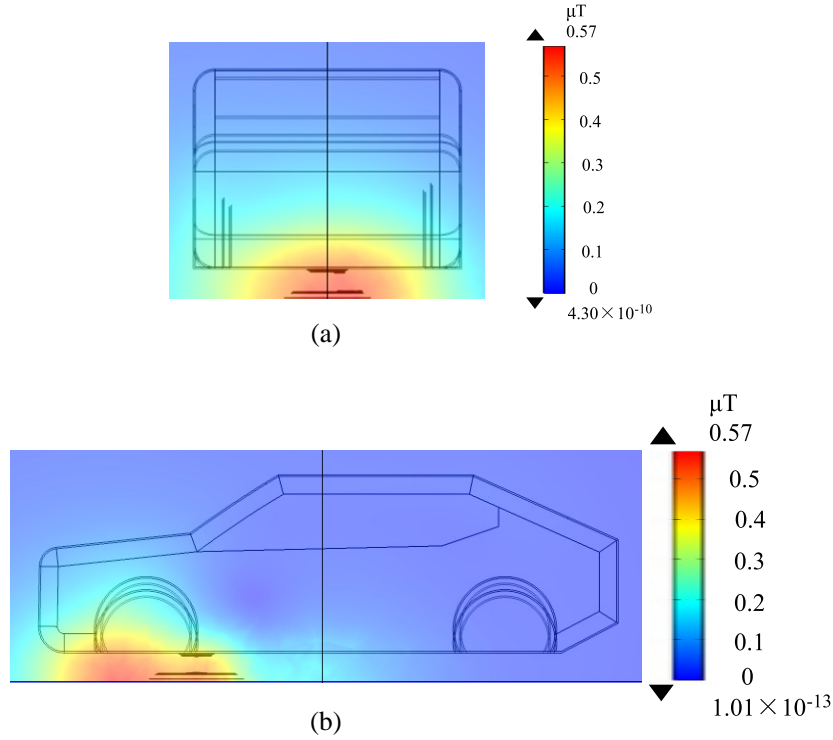


Figure 8. Magnetic field distributions around the wireless charging EV on (a) the $Y - Z$ plane (front view) and (b) the $X - Z$ plane (left view) when the GA and VA aligned.

The red line 1 in Fig. 5(a) is the bottom boundary of the $Y\text{-}Z$ plane. The value of magnetic flux densities calculated on line 1 at different offset distances in the X -axis and Y -axis are shown in Fig. 9. Fig. 9(a) shows that when the offset only happens in the forward and backward directions, the value of magnetic flux density significantly increases with the increase in offset distance. Similarly, the larger the offset distance is in the lateral direction, the larger the corresponding electromagnetic field is. In addition, the increase of the magnetic field on the side of the direction of movement of the GA is not very significant.

In this study, the worst-case coil distance ($Z1 = 130\text{ mm}$) and offset ($\Delta X = 100\text{ mm}$ and $\Delta Y = 75\text{ mm}$) were set. Fig. 9 presents the magnetic field distribution under the worst-case condition.

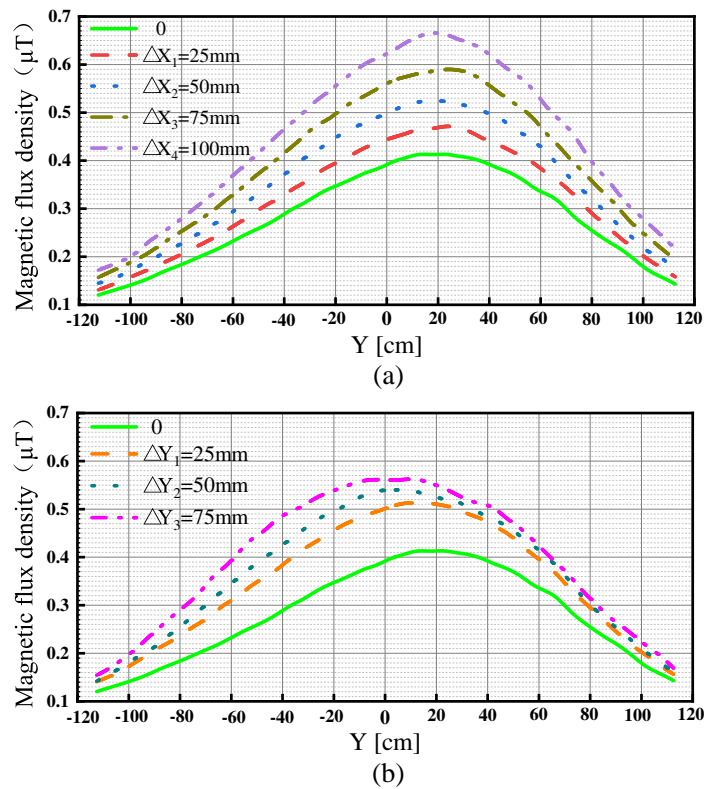


Figure 9. Magnetic flux density B is calculated on line 1 at different offset distances in (a) the fore and aft direction (X axis) and lateral direction (Y axis).

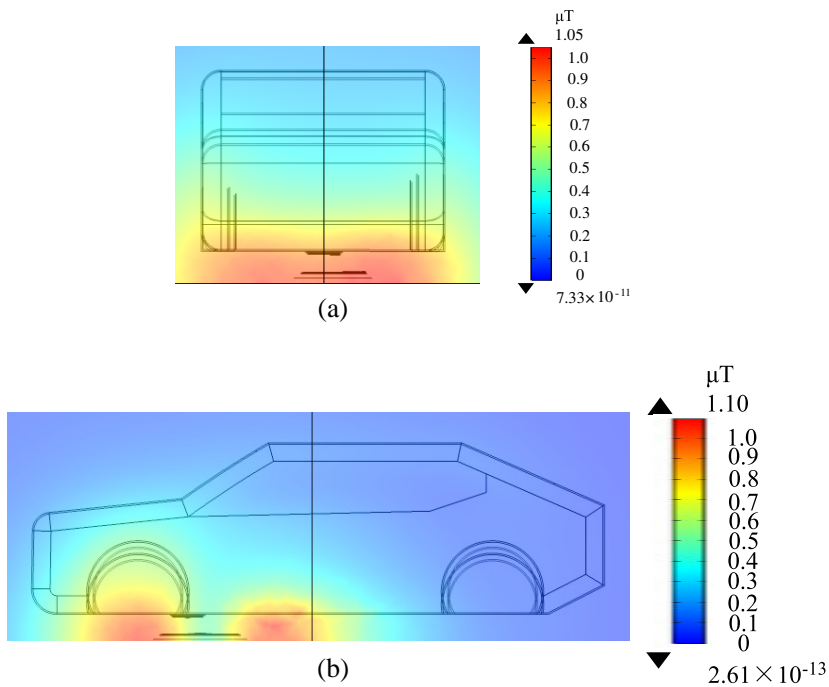


Figure 10. Magnetic flux density distributions around the wireless charging EV on (a) the Y-Z plane (front view) and (b) the X-Z plane (left view) under the worst-case case.

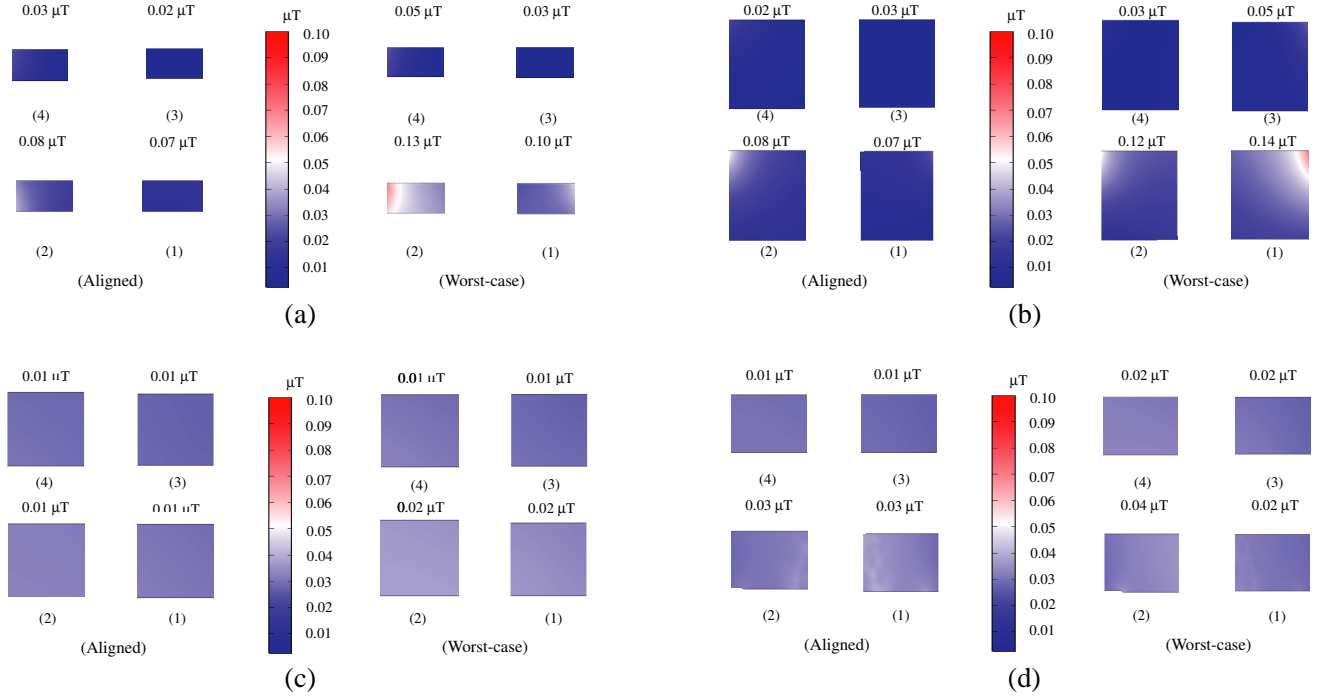


Figure 11. Magnetic flux density distributions inside the wireless charging EV on (a) the head, (b) the chest, (c) the seat cushion, and (d) the foot under different cases.

It can be determined that the dislocation results in a distortion of the external magnetic flux density in the direction of the dislocation, as shown in Fig. 10(b) compared with Fig. 8(b). In this case, although the maximum lateral offset leads to a significant increase in the magnetic flux density compared to the alignment case, up to $1.1 \mu\text{T}$ in the X - Z plane, it still meets the EMF safety limits.

The magnetic flux density distributions inside the wireless charging EV on the head, chest, seat cushion, and foot for the two considered test cases are shown in Fig. 11. The value of magnetic fields inside the EV is much lower than outside, which is consistent with the findings in Section 4.1, and the maximum magnetic flux density occurs at the chest of the driver's seat under the worst operating conditions, with a value of $0.14 \mu\text{T}$. The reason for this result is that no specific material properties have been set for the window components, and thus, the electromagnetic shielding at the windows is very poor.

Therefore, the EMF safety limit in ICNIRP Guidelines was never exceeded around or inside the wireless charging EV in all considered cases.

5. CONCLUSION AND FURTHER WORK

In this paper, the electromagnetic safety performance of an EV equipped with a 7.7 kW WPT system recommended by GB/T 38775 (in Chinese) is investigated by a numerical procedure. Different working conditions have been set, one for GA and VA alignment and the other for the misalignment case, i.e., the worstcase is $\Delta X = 100 \text{ mm}$ and $\Delta Y = 75 \text{ mm}$, based on the proposals for standardization. The coupler misalignment leads to an increase of magnetic field leakage, reaching the maximum magnetic flux densities of $1.1 \mu\text{T}$ and $0.14 \mu\text{T}$ on the X - Z plane and the in-car seat test plane, respectively, in the worst-case scenario. The comparison results demonstrate that, in both the alignment and worst-case situations, the electromagnetic fields inside or outside the EV meet the ICNIRP limits. Therefore, the 7.7 kW WPT system discussed in this paper has good safety performance in the electromagnetic environment.

The research in this paper also gives a solution for the prediction of EMF safety for wireless charging of EVs under a worst-case scenario and has a certain reference value.

ACKNOWLEDGMENT

This work was funded by the State Grid Corporation of China and the research project number is 5200-202113091A-0-0-00.

REFERENCES

1. Patil, D., M. K. McDonough, J. M. Miller, B. Fahimi, and P. T. Balsara, "Wireless power transfer for vehicular applications: overview and challenges," *IEEE Trans. Transp. Electrification*, Vol. 4, No. 1, 3–37, Mar. 2018.
2. Sun, L., D. Ma, and H. Tang, "A review of recent trends in wireless power transfer technology and its applications in electric vehicle wireless charging," *Renew. Sust. Energ. Rev.*, Vol. 91, 490–503, Aug. 2018.
3. Vaka, R. and R. k. Keshri, "Review on contactless power transfer for electric vehicle charging," *Energies*, Vol. 10, No. 5, 636, May 2017.
4. Garnica, J., R. A. Chinga and J. Lin, "Wireless power transmission: from far field to near field," *Proc. IEEE*, Vol. 101, No. 6, 1321–1331, Jun. 2013.
5. Mahesh, A., B. Chokkalingam, and L. Mihet-Popa, "Inductive wireless power transfer charging for electric vehicles—a review," *IEEE Access*, Vol. 9, 137667–137713, Sep. 2021.
6. Mou, X., D. T. Gladwin, R. Zhao, and H. Sun, "Survey on magnetic resonant coupling wireless power transfer technology for electric vehicle charging," *IET Power Electron.*, Vol. 12, No. 12, 16, Oct. 2019.
7. Liu, J., X. Zhang, J. Yu, Z. Xu, and Z. Ju, "Performance analysis for the magnetically coupled resonant wireless energy transmission system," *Complexity*, Vol. 2019, 1–13, Nov. 2019.
8. *Wireless Power Transfer for Light-Duty Plug-in/Electric Vehicles and Alignment Methodology*, SAE J2954, Oct. 2020.
9. Andre, K., K. Aresteidis, M. Robert, J. D. Joannopoulos, P. Fisher, and M. Soljacic, "Wireless power transfer via strongly coupled magnetic resonances," *Science (New York, N.Y.)*, Vol. 317, No. 5834, 83–86, Jul. 2007.
10. Campi, T., S. Cruciani, F. Maradei, and M. Feliziani, "Magnetic field during wireless charging in an Electric Vehicle according to standard SAE J2954," *Energies*, Vol. 12, No. 9, 1795–1819, May 2019.
11. *Electrically Propelled Road Vehicles — Magnetic Field Wireless Power Transfer — Safety and Interoperability Requirements*, ISO 19363, Apr. 2020.
12. *Electric Vehicle Wireless Power Transfer: Part 4, Limits and Test Methods of the Electromagnetic Environment*, GB/T 38775.4-2020 (in Chinese), Apr. 2020.
13. *Electric Vehicle Wireless Power Transfer (WPT) System: Part 1, General Requirements*, IEC 61980-1, Nov. 2020.
14. International Commission on Non-Ionizing Radiation Protection (ICNIRP), "Guidelines for limiting exposure to time-varying electric and magnetic fields (1 Hz to 100 kHz)," *Health Phys.*, Vol. 99, No. 6, 818–836, Dec. 2010.
15. Park, S., "Evaluation of electromagnetic exposure during 85 kHz wireless power transfer for electric vehicles," *IEEE Trans. Magn.*, Vol. 54, No. 1, 1–8, Jan. 2018.
16. Santis, V. D., T. Campi, S. Cruciani, S. Laakso, and M. Feliziani, "Assessment of the induced electric fields in a Carbon-Fiber electrical vehicle equipped with a wireless power transfer system," *Energies*, Vol. 11, No. 3, 684–693, Mar. 2018.
17. Mou, W. and M. Lu, "Research on shielding and electromagnetic exposure safety of an electric vehicle wireless charging coil," *Progress In Electromagnetics Research*, Vol. 117, 55–72, Dec. 2021.
18. *Electric Vehicle Wireless Power Transfer: Part 6, Interoperability Requirements and Testing — Ground Side*, GB/T 38775.6-2021 (in Chinese), Oct. 2021.
19. *Electric Vehicle Wireless Power Transfer: Part 7, Interoperability Requirements and Testing — Vehicle Side*, GB/T 38775.7-2021 (in Chinese), Oct. 2021.

20. Jiang, C., K. T. Chau, C. Liu, and C. H. T. Lee, “An overview of resonant circuits for wireless power transfer,” *Energies*, Vol. 10, No. 7, 894, Jun. 2017.
21. Campi, T., S. Cruciani, F. Maradei, and M. Feliziani, “Near-field reduction in a wireless power transfer system using LCC compensation,” *IEEE Trans. Electromagn. Compat.*, Vol. 59, No. 2, 686–694, Apr. 2017.
22. Shen, D., G. Du, W. Zeng, Z. Yang, and J. Li, “Research on optimization of compensation topology parameters for a wireless power transmission system with wide coupling coefficient fluctuation,” *IEEE Access*, Vol. 8, 59648–59658, Apr. 2020.
23. Liu, J., X. Zhang, J. Yu, Z. Xu, and Z. Ju, “Performance analysis for the magnetically coupled resonant wireless energy transmission system,” *Complexity*, Vol. 2019, 1–13, Nov. 2019.